Astron. Astrophys. 209, 361–368 (1989)

ASTRONOMY AND ASTROPHYSICS

A study of the composite supernova remnant G 18.95-1.1

E. Fürst [1], E. Hummel [1,*], W. Reich [1], Y. Sofue [2,3], W. Sieber [1], K. Reif [4], and R.-J. Dettmar [4,]**

[1] Max-Planck-Institut für Radioastronomie, Auf dem Hügel 69, D-5300 Bonn 1, Federal Republic of Germany
[2] Nobeyama Radio Observatory, Minamimaki-mura, Minamisaku-gun, Nagano 384-13, Japan
[3] Department of Astronomy, University of Tokyo, Bunkyo-ku, Tokyo 113, Japan
[4] Radioastronomisches Institut der Universität Bonn, Auf dem Hügel 71, D-5300 Bonn 1, Federal Republic of Germany

Received May 26, accepted July 30, 1988

Summary. The galactic nonthermal object G 18.95–1.1 has a spectral index of $\alpha = -0.28$ ($S_\nu \propto \nu^\alpha$) between 57.5 MHz and 10 GHz. About 80% of its emission is diffuse or unresolved at arcmin resolution and peaks at the centre of the source. 20% of its emission is found in arc like features, which have a slightly steeper spectrum compared with the diffuse emission, except for the central structure, which has a somewhat flatter spectrum. The morphology and the spectral characteristics of G 18.95–1.1 classify it as a composite supernova remnant.

H I line data shown a depression in antenna temperature of the extent of G 18.95–1.1 at 18 km s^{-1} giving a distance of 2 kpc. The physical size of G 18.95–1.1 is 20 pc and its luminosity is about 6 10^{33} erg s^{-1}. Observations with the Very Large Array at 1.49 GHz and 4.9 GHz with arcsec angular resolution confirm the spectral index differences between the central arc and the outer arc structures. Morphologically, the central feature resembles a two-sided radio jet, but shows no central compact source. Optical data did not show any particular star like object near the centre of G 18.95–1.1. A search for a pulsar at 1.61 GHz using the Effelsberg 100 m telescope was unsuccessful.

Key words: radio continuum emission – supernova remnants – H I line emission

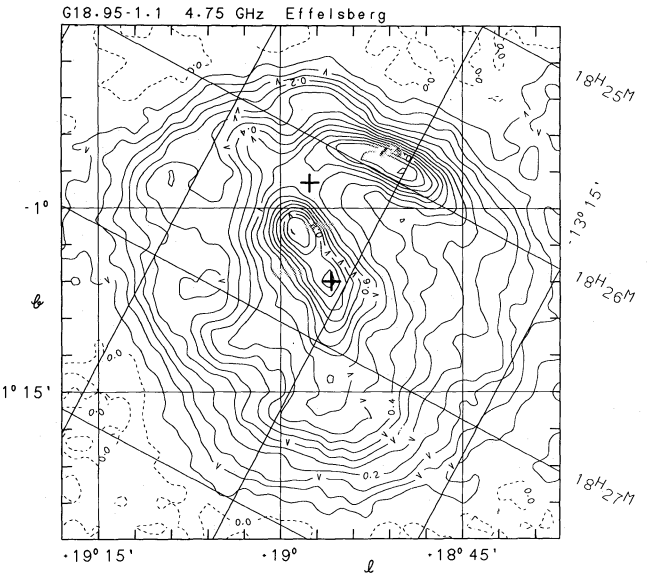

Fig. 1. Contour plot of G 18.95–1.1 at 4.75 GHz. Contours are shown in steps of 50 mK T_B. The half power beam width is 2'.45. The crosses denote the positions at which we searched for a pulsar (see Sect. 4)

1. Introduction

During the systematic radio continuum observations of objects in the galactic plane Fürst et al. (1985) discovered the nonthermal nature of the galactic source G 18.95–1.1. From the brightness distribution of this object (Fig. 1) it is apparent that G 18.95–1.1 consists of various arcs pointing towards the radio peak near its geometrical centre. This morphology suggests a central activity. Stimulated by an investigation of G 357.7–0.1 and G 5.3–1.0 by Helfand and Becker (1986) Fürst et al. proposed an accreting binary system as the energy source of G 18.95–1.1. Odegard (1986) suggested a central pulsar as an alternative interpretation. If the magnetic and rotational axes of this pulsar are closely aligned, ordered magnetic beams containing relativistic particles are expected (Benford, 1984). These beams may be represented by the central bar-like feature and the bright slightly curved western arc. A problem of this model is the explanation of the weaker arcs (Odegard, 1986). Faced with the available observations no proposed model can be considered as conclusive.

The classification of G 18.95–1.1 as a nonthermal object is based on radio continuum observations between 1.42 GHz and 10 GHz (Fürst et al., 1985). The radio spectral index was found to be $\alpha = -0.4 \pm 0.2$ ($S_\nu \propto \nu^\alpha$), while the object shows weak polarization at 4.75 GHz ($\approx 2.5\%$). Additional observations at 57.5 MHz using the Clark Lake synthesis telescope were reported by Odegard (1986). The radio continuum data between 57.5 MHz and 5 GHz can be fitted by a power law with spectral index $\alpha = -0.28 \pm 0.05$. Odegard also found a slight variation of α across the source: the spectrum of the central part seems to be flatter than the outer regions. Recently, Patnaik et al. (1988)

Send offprint requests to: E. Fürst

* Present address: Nuffield Radio Astronomy Laboratories, Jodrell Bank, Macclesfield, Cheshire SK 11 9DL, U.K.

** Visiting Astronomer at the ESO/MPI 2.2 m telescope, La Silla, Chile

reported radio observations of G 18.95–1.1 at 327 MHz with the Ooty synthesis radio telescope (OSRT). These authors also found a slight spectral steepening of about $\Delta\alpha \approx 0.15$ from the centre towards the northwestern shell. Their radio map does not show the arc-like structures, particularly in the east of G 18.95–1.1, as observed by Fürst et al. (1985, see Fig. 1).

Although several new observations were added in the last two years, the morphology of G 18.95–1.1 is still unclear, as is the nature of the central feature and the outer arcs or shells. In this paper we, therefore, present a more detailed analysis of the radio data reported by Fürst et al. (1985). In addition, we report on new observations at 1.49 and 4.9 GHz using the Very Large Array (VLA) in the C and D configurations and on a search for a pulsar with the 100 m telescope at 1.61 GHz at two selected positions. In addition we inspected optical data for peculiar star-like objects. We have also analysed observations in the H I line at 1.42 GHz reported by Braunsfurth and Rohlfs (1984) with the 100 m telescope in order to derive the istance to G 18.95–1.1. A first short comment on these data was given by Fürst et al. (1987).

2. Radio continuum observations of G 18.95–1.1

2.1. Analysis of the radio data at 2.695 GHz, 4.75 GHz, and 10 GHz

The radio observations at 2.695 GHz, 4.75 GHz, and 10 GHz were obtained as part of a systematic investigation of galactic objects. A detailed description of this procedure is given by Reich et al. (1986). It is apparent from the 4.75 GHz map, which has the highest angular resolution, that two components contribute to the radio emission of G 18.95–1.1: A large-scale diffuse component and several arc-like features. This is best seen when the large-scale diffuse component is filtered out using the "background filtering" method developed by Sofue and Reich (1979). The decomposition, using a filtering beam of 3'.5, is shown in Fig. 2 (large-scale component) and in Fig. 3 (small-scale component). The integrated flux density of the diffuse component is $S \approx 18.8$ Jy 4.75 GHz ($\approx 80\%$ of the total flux density of $S = 23.8$ Jy). The arc-like features, shown in Fig. 3, have an integrated flux density of $S \approx 5$ Jy. The most prominent features are the bright north-western arc (running from $l = 18°55'$, $b = -0°55'$ to $l = 18°45'$, $b = -1°00'$) and the central feature running from $l = 19°00'$, $b = -1°00'$ to $l = 18°55'$, $b = -1°10'$. Also noticeable are the prominent arcs in the eastern part of the source. The arc running from $l = 19°00'$, $b = -1°10'$ to $l = 19°10'$, $b = -1°05'$ is not visible in the 327 MHz radio map observed by Patnaik et al. (1988). Probably the sensitivity of the 327 MHz map is insufficient to detect this faint arc.

The radio maps at 2.695 GHz, 4.75 GHz, and 10 GHz were convolved to a circular beam with a HPBW of 4'.3, and subsequently separated into the arc-like structures and the large-scale diffuse component using a 5' circular filtering beam. At all three frequencies the diffuse component contains $80 \pm 3\%$ of the total emission. The calculation of spectral indices using integrated flux density values normally suffers from the uncertainties of the relative zerolevels. Therefore, differential spectral index plots (TT-plots, see Turtle et al., 1962) were performed. The spectral indices obtained with this method are less dependent on remaining background emission. For the total emission of G 18.95–1.1 we obtained a spectral index of $\alpha_{tot} = -0.28 \pm 0.02$ for all combinations of the three maps. This constancy implies that obviously the integrated flux density value at 10 GHz given by Fürst et al. (1985) is too low, likely due to some missing weak extended emission. The spectral index α_{tot} agrees very well with the value obtained by Odegard (1986). For the diffuse component (Fig. 2) we obtained $\alpha_{diff} = -0.27 \pm 0.03$ and for the arc-like feature (Fig. 3) $\alpha_{arc} = -0.40 \pm 0.15$. Separately, we investigated the spectral indices of the central feature and the bright north-western arc. For the central feature we obtained $\alpha_c = -0.26 \pm 0.05$, for the north-western arc $\alpha_a = -0.35 \pm 0.05$. We conclude from these results: Within the errors the spectral indices of all components are equal. However, there is a slight tendency that the north-western arc has a steeper spectrum ($\Delta\alpha \approx 0.1$) than the central feature and the large-scale diffuse component. For the eastern arc the spectral index is $\alpha = -0.5 \pm 0.2$, i.e. the emission is nonthermal but the spectral index is not well determined. The slight variation of the

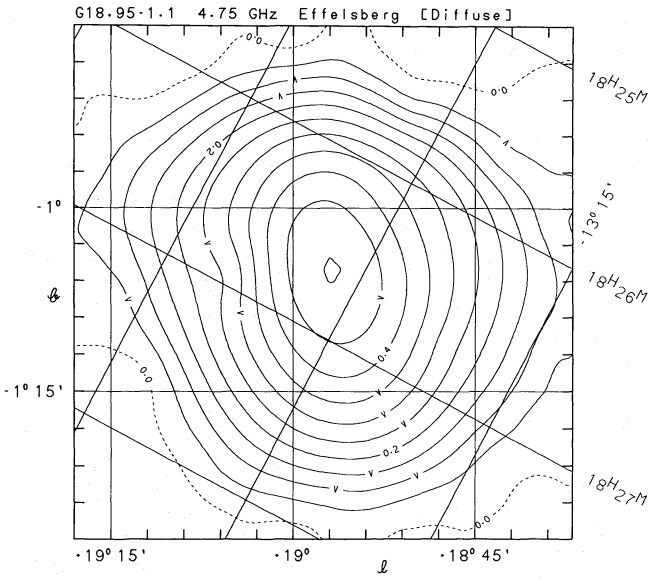

Fig. 2. Contour plot of the large-scale, diffuse component of G 18.95–1.1 at 4.75 GHz. Contours are shown in steps of 50 mK T_B. The half power beam width is 2'.45

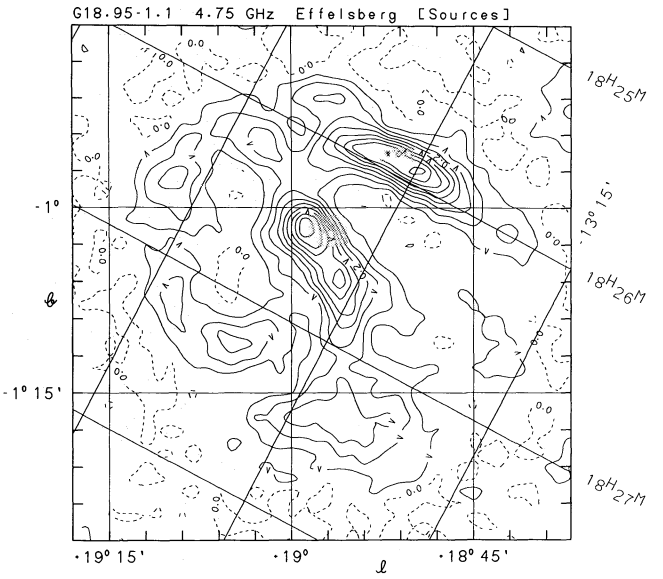

Fig. 3. Contour plot of the small-scale structure of G 18.95–1.1 at 4.75 GHz. Contours are shown in steps of 50 mK T_B. The half power width is 2'.45

spectral index between the central feature and the north-western arc agrees with the results reported by Odegard (1986) and Patnaik et al. (1988).

2.2. *Radio continuum observations at 1.49 GHz and 4.9 GHz with the VLA*

In order to study the morphology of G 18.95–1.1 in more detail we observed its radio continuum emission with the Very Large Array (VLA) in its C and D configurations at 1.49 GHz and 4.9 GHz. At both frequencies the observations were done with two independent IFs, each with a bandwidth of 50 MHz and separated by 50 MHz. The 4.9 GHz D-configuration observations were done at two positions to cover the predominant features in the north-west and near the centre. Some important observational parameters are given in Table 1. During the reduction we noticed a too high noise in the polarization data at both frequencies, probably due to the relatively short observing time. The following is restricted to total intensity only.

The edited and calibrated visibility data were Fourier transformed to obtain maps of the total intensity. In the map-making procedure the side-lobes of the synthesized beam were removed. As expected we miss large-scale structures in all maps. This causes deep negative bowls in the maps which could not adequately be removed by the "cleaning" process. We made several attempts to improve on the problem by implementing a zero spacing flux (from the single dish measurements) with various weights. Because of the complicated source structure this did not improve the maps. Subsequently, the discussion here concerning the VLA data is limited to the small-scale morphology and can only be qualitative.

In Fig. 4 we show the 1.49 GHz contour map (D- and C-array UV-data concatenated and not corrected for the primary beam attenuation). The map has been convolved to a circular beam of HPBW = 45″ and the rms noise is ≈0.1 mJy/beam. This map shows the arc-like features. Because of the missing short spacings we are insensitive to structures > 7′.6. The main structures visible

Table 1. Observational parameters of the radio continuum observations at 1.49 GHz and 4.9 GHz with the Very Large Array (VLA)

Configuration	C		D[1]	
Date of observation	Aug. 31, 1985		Dec. 27, 1985	
Right ascension (1950)	$18^h26^m31^s$		$18^h26^m33^s$	
Declination (1950)	-12°59'05"		-12°57'00"	
Frequency [GHz]	1.49	4.86	1.49	4.86
Bandwidth [MHz]	100		100	
Longest spacing [km]	3.4		1.0	
Shortest spacing [m]	63		40	
Missing large-scale structure[2] [arcmin]	4.8	1.5	7.6	2.3
Primary beam half power full width [arcmin]	31	9	31	9
Amplitude calibrator	3C286		3C286	
Calibrator flux density [Jy][3]	14.39	7.44	14.39	7.44
Phase calibrator	1741-038		1741-038	
Observing time [h]	1.2	1.5	1.0	2x1.0

[1] A second observation at 4.86 GHz was done at R.A. = $18^h25^m57^s$ and Decl. = -12°56'20" (1950.0)

[2] Gaussian brightness distribution with a half power size as given have a visibility of 0.5

[3] Based on the Baars et al. (1977) scale

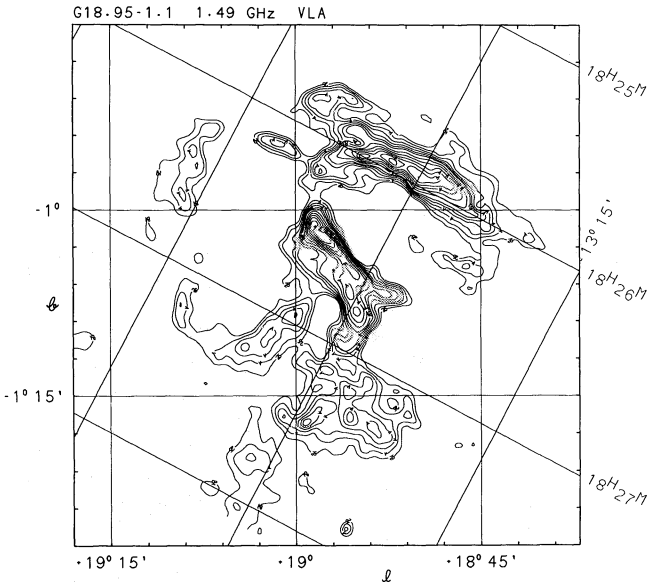

Fig. 4. Contour plot of G 18.95–1.1 at 1.49 GHz observed with the Very Large Array (C- and D-UV-data concatenated). The map is not corrected for the primary beam attenuation and is convolved to a circular half power beam width of 45″. The rms noise is 0.1 mJy/beam. Contours are shown in steps of 2.5 mJy/beam up to 15 mJy/beam and further on in steps of 5 mJy/beam

in this map are also seen in the 4.75 GHz observation with the Effelsberg 100 m telescope, in particular when the large-scale structures are filtered out (Fig. 3). In contrast to the radio map at 327 MHz (Patnaik et al., 1988), the arc-like features visible in the 4.75 GHz (Fig. 3) and in the 1.49 GHz (Fig. 4) maps are almost identical.

In Fig. 5 we show the higher resolution maps obtained with the VLA in its C and D configurations at 1.49 GHz and 4.9 GHz, respectively. The maps obtained at 4.9 GHz at the two positions given in Table 1 were corrected for the primary beam attenuation and combined. The 1.49 GHz map shown in Fig. 5 is also corrected for the primary beam attenuation. Both maps have an HPBW = 19″×14″ (p.a. = 0°) and the rms noise is 1.0 and 0.5 mJy/beam at 1.49 GHz and 4.9 GHz, respectively. At some positions we determined the spectral index between 1.49 GHz and 4.9 GHz (shown in the upper panel of Fig. 5). Because of the bowl-shaped, negative zerolevel we had to determine the zerolevel locally and because the missing large-scale structure is not exactly the same for both frequencies the absolute value of the spectral indices are not precisely known. Since we do miss slightly more structure at 4.9 GHz we suspect our spectral indices to be too low (i.e. the radio spectra are probably flatter). However, the systematic difference between the eastern and the western ridge in Fig. 5 is real. The formal errors, neglecting the systematic errors caused by missing large-scale structure, in the spectral indices is ±0.05. In addition, we performed TT-plots for each feature separately and obtained $\alpha_e = -0.52 \pm 0.06$ for the eastern ridge (central feature of G 18.95–1.1) and $\alpha_a = -0.68 \pm 0.05$ for the western ridge. Again, important is the difference between the two values, indicating that the radio spectra of both features are different.

The higher angular resolution map we obtained is shown in Fig. 6. It shows the central feature of G 18.95–1.1 at 4.9 GHz with a resolution of 6″. The cleaned map has a rms noise of 0.06 mJy/beam. The map is superposed on a blue print of the Palomar Sky Survey Plates.

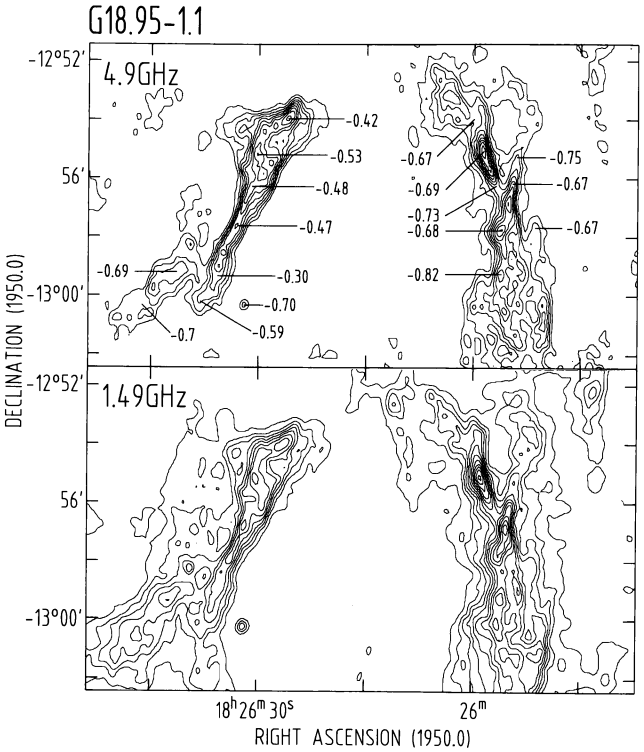

Fig. 5. Contour plot of a part of G 18.95–1.1 at 4.9 GHz (upper panel, contour steps 0.5 mJy/beam) and at 1.49 GHz (lower panel, contour steps 1.0 mJy/beam) obtained with the Very Large Array (C and D configuration). Both maps are corrected for the primary beam attenuation. The half power beam width is $19'' \times 14''$ (p.a. $= 0°$) in both maps. In the upper panel some spectral indices $\alpha (S_\nu \propto \nu^\alpha)$ are quoted. The rms noise is 0.5 mJy/beam and 0.2 mJy/beam respectively

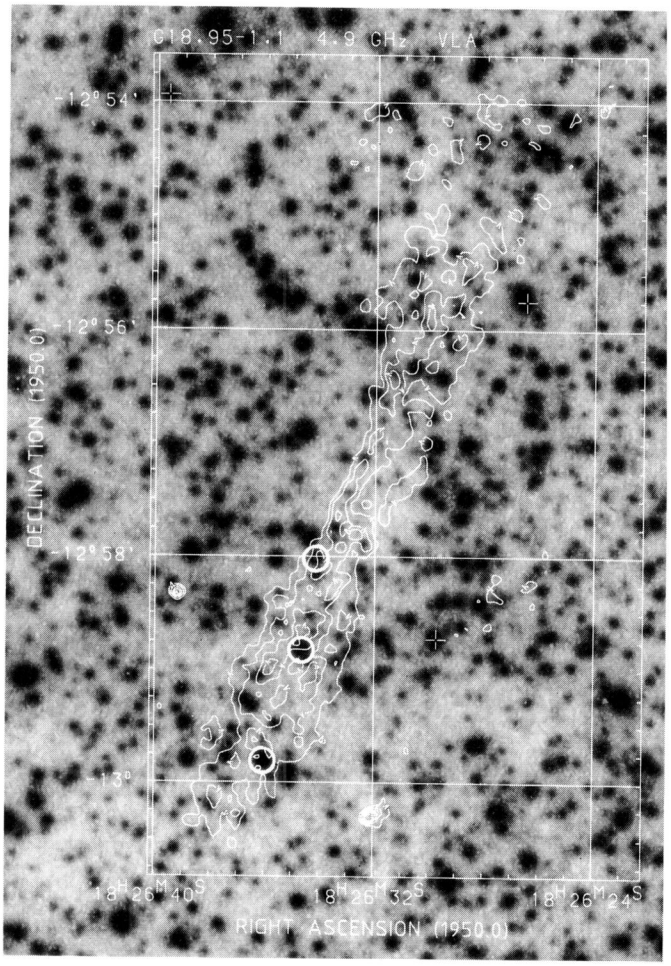

Fig. 6. Contour plot of the central feature of C 18.95–1.1 at 4.9 GHz observed with the Very Large Array (C-configuration) superposed on the Palomar blue print. The contour steps are 0.15 mJy/beam, the rms noise is 0.06 mJy/beam. The half power beam width is 6″. Circles denote stellar objects which have been observed spectroscopically

3. Observations of the H I 21 cm line

G 18.95–1.1 is located in an area which has been observed in the H I line at 21 cm wavelength with the 100 m telescope by Braunsfurth and Rohlfs (1984). These data were obtained using the frequency switching method at a sampling interval of 6′ and $2\,\mathrm{km\,s^{-1}}$. A sensitivity of $\Delta T_A = 0.5\,\mathrm{K}$ (T_A = antenna temperature) was obtained. The conversion factor between T_A and the brightness temperature T_B was $T_B/T_A = 1.2$ and the angular resolution was 9′.

Inspecting the channel maps near G 18.95–1.1 we found a depression of $\Delta T_B = 12\,\mathrm{K}$ at a radial velocity of $18\,\mathrm{km\,s^{-1}}$ centered on the position of the radio continuum peak of G 18.95–1.1 (see Fig. 1). In Fig. 7 we show channel maps between the radial velocities $v = 10\,\mathrm{km\,s^{-1}}$ and $v = 26\,\mathrm{km\,s^{-1}}$. The centre of the depression is near galactic longitude $l = 19°$ and latitude $b = -1°$. The extent of the depression in radial velocity is $\Delta v = 8\,\mathrm{km\,s^{-1}}$. In Fig. 8 we show the H I channel map at the radial velocity $v = 18\,\mathrm{km\,s^{-1}}$ and the outer boundary (40 mK T_B contour of Fig. 1) of G 18.95–1.1. The good positional coincidence of the H I depression and G 18.95–1.1 is evident. This is also demonstrated by galactic longitude and latitude scans in the H I line emission intersecting at $l = 18.^{\circ}9$ and $b = -1°$ as shown in Fig. 9. In longitude the scan represents the original data at a radial velocity $v = 18\,\mathrm{km\,s^{-1}}$ ($\pm 1\,\mathrm{km\,s^{-1}}$). The latitude scan is shown after subtraction of a linear baseline in order to reduce the influence by the steep temperature gradient in galactic latitude. The centre of the depression coincides well with the intensity peak of G 18.95–1.1. The peak brightness temperature in the radio continuum at 1.42 GHz as observed with the 100 m telescope is $T_B \approx 6.5\,\mathrm{K}$.

The H I depression may be explained by the absorption of a cloud of H I gas in front of G 18.95–1.1. In this case the depression can be calculated from $\Delta T_B \approx (T_B^B - T_{CL})\,(1 - \exp(-\tau)) - T_B^C \exp(-\tau)$, where T_B^B is the brightness temperature of the H I-background emission (about 63 K $T_B/T_A \approx 75.6\,\mathrm{K}$, see the plateau in the longitude scan in Fig. 9 east of the depression), T_B^C is the peak radio continuum brightness temperature at 1.42 GHz ($\approx 6.5\,\mathrm{K}$), T_{CL} is the spin temperature of the H I cloud, and τ is its optical depth. We obtain $\tau = 0.4$ for $T_{CL} = 30\,\mathrm{K}$ and $\tau = 0.9$ for $T_{CL} = 50\,\mathrm{K}$. However, the apparent sizes of the H I cloud and G 18.95–1.1 must be very similar, and such a chance coincidence is unlikely. The absorbing H I cloud should have a H I column

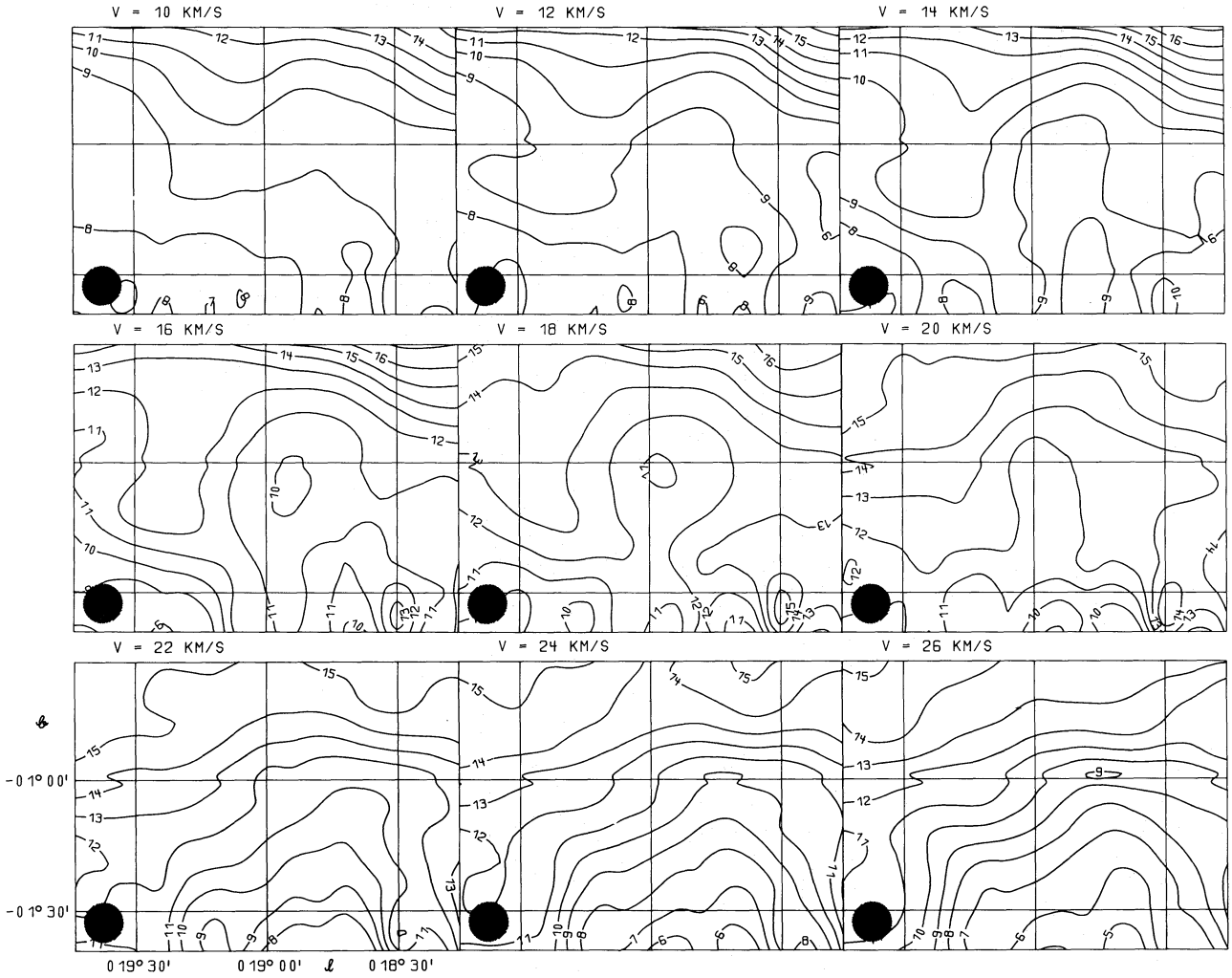

Fig. 7. Contour plot of the H I 21 cm line channel maps obtained with the Effelsberg 100 m telescope. The contour steps are 5 KT_A beginning at 2 KT_A (contour 1). The plots show radial velocities between 10 km s^{-1} and 26 km s^{-1} at an interval of 2 km s^{-1}. The half power beam width is 9′ as is indicated by the hatched circles

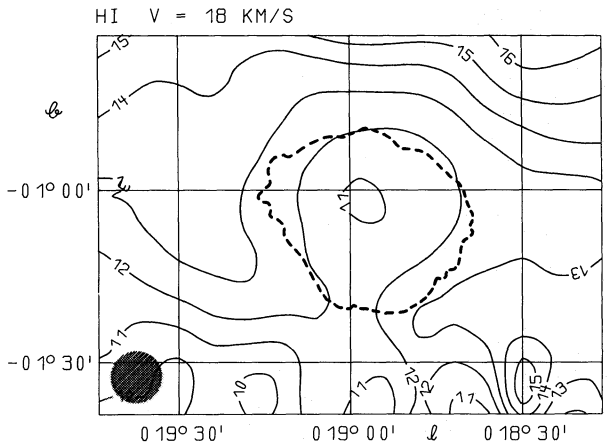

Fig. 8. Enlargement of the central map of Fig. 7. Superposed is the outer boundary of G 18.95–1.1. Contours are the same as in Fig. 7

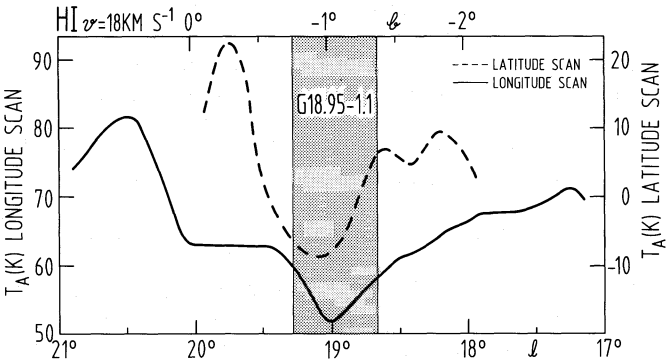

Fig. 9. Longitude and latitude scans across G 18.95–1.1 in the H I-21 cm line antenna temperature. The scans intersect at $l = 18.^{\circ}9$, $b = -1°$. The latitude scan is shown after subtraction of the large scale galactic temperature gradient. The shaded area denotes the relative position of G 18.95–1.1

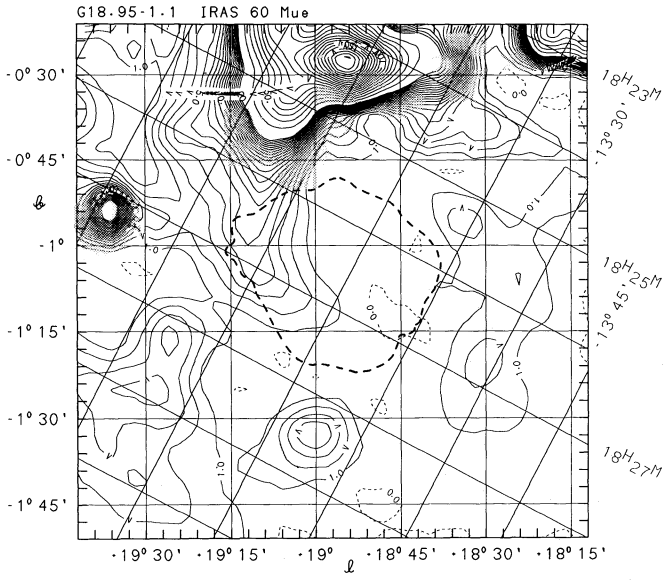

Fig. 10. Contour plot of the IRAS 60 μ emission after removing the galactic emission gradient. The contour steps are 1000 Jy/ster beginning at 0 Jy/ster up to 20000 Jy/ster and further on in steps of 10000 Jy/ster. The half power beam width is ≈5′. Superposed is the outer boundary of G 18.95–1.1

density of $>10^{20}\,\mathrm{cm}^{-2}$. A good correlation between the H I column density and the far-infrared emission was found by Boulanger et al. (1985). In Fig. 10 we show the far-infrared map at 60 μm obtained with the far-infrared satellite (IRAS, Beichman et al., 1984). The galactic emission gradient was removed using the "background-filtering"-method (see Sect. 2.1). At the position of the H I depression and G 18.95–1.1 there is no enhanced emission which could be associated with the absorbing H I gas. Obviously, an absorbing cloud in front of G 18.95–1.1 as the cause of the H I depression is very unlikely.

More probably, the H I depression is caused by a cavity in the interstellar H I distribution. The perfect positional coincidence of the centres of the H I depression and the continuum sources makes a chance coincidence hard to believe. The missing column density can be estimated from $\langle \Delta N(\mathrm{cm}^{-2})\rangle = 1.823\ 10^{18} \int \Delta T_B(v)\, dv$ (Kerr, 1968). We obtained $\langle \Delta N(\mathrm{cm}^{-2})\rangle \simeq 9\ 10^{19}$, assuming $\Delta T_B = 12\,\mathrm{K}$ and a half width in radial velocity of $\Delta v = 4\,\mathrm{km\,s}^{-1}$.

If we assume a physical relation between the H I depression and G 18.95–1.1, we may estimate the distance to G 18.95–1.1 from the radial velocity $v = 18\,\mathrm{km\,s}^{-1}$. According to Einasto (1978), Schmidt (1965) and Ostriker and Caldwell (1978) we obtain $d \approx 2$ kpc or $d \approx 15$ kpc on the far side of our Galaxy. The linear size of G 18.95–1.1 is then calculated to $D = 20$ pc (distance from the galactic plane $z \approx 36$ pc) and $D = 160$ pc ($z \approx 290$ pc), respectively. However, the large distance is very unlikely. At a distance of 15 kpc G 18.95–1.1 would have a luminosity of $L(10^7$–$10^{11}\,\mathrm{Hz}) \approx 4\ 10^{35}\,\mathrm{erg\,s}^{-1}$, more than twice the luminosity of the Crab nebula. Such bright objects should be very young. For an age of 10^3 yr and free expansion an expansion velocity of $v \approx 75000\,\mathrm{km\,s}^{-1}$ is necessary, more than thirty times the expansion velocity of the Crab nebula. Obviously, at the large distance of 15 kpc, G 18.95–1.1 would be a very unusual nonthermal galactic object. Therefore, we prefer a distance of $d = 2$ kpc, placing G 18.95–1.1 within the Sagittarius arm.

The radio continuum surface brightness at 1 GHz is $\Sigma_{1\,\mathrm{GHz}} \approx 4.4\ 10^{-21}\ (\mathrm{W\,m}^{-2}\,\mathrm{Hz}^{-1}\,\mathrm{sr}^{-1})$ assuming $S_{1\,\mathrm{GHz}} = 36$ Jy and an apparent size of 35′. If we apply the $\Sigma - D$ relations by Clark and Caswell (1976), Milne (1979) and Berkhuijsen (1983) we obtain a distance between 3.5 kpc and 7.1 kpc. The $S\theta^2 - d$ relation for filled-center SNRs (Weiler and Panagia, 1980) yields 3.0 kpc. These distances are somewhat larger than the 2 kpc derived from the H I line data and significantly smaller than 15 kpc. In the following we assume a distance of 2 kpc.

At a distance of 2 kpc ($D = 20$ pc) the column density $\langle \Delta N\rangle$ derived above corresponds to a density of $N = 1.5\,\mathrm{cm}^{-3}$. G 18.95–1.1 has expanded into a medium of density $N \geqq 1.5\,\mathrm{cm}^{-3}$.

4. Search for a compact central source

As a first step, we made a search for a radio pulsar at two positions near the centre of G 18.95–1.1 with the 100 m telescope at Effelsberg. The observations were done on 15.04.1986 at the frequency 1.61 GHz (HPBW = 7′.8). The first position at $l = 18°57'00''$, $b = -0°57'20''$ (see Fig. 1) was chosen between the central bar-like feature and the north-western arm assuming that a pulsar may power both features. The second position was at $l = 18°55'00''$, $b = -1°06'00''$, south-west of the centre of the bar-like structure. Because of the large HPBW the observations at these two positions covered most of the inner portion of G 18.95–1.1.

If a pulsar is located inside G 18.95–1.1, this object would have the signature of a Crab-like SNR. The pulsar associated with the Crab nebula has an age of 933 yr and a period of $P = 33$ ms (Manchester and Taylor, 1981), while the much older Vela X pulsar (age 40000 yr) has a period of 88 ms. Since the age of G 18.95–1.1 is probably a few 10^3 yr (see Sect. 5) we searched for a pulsar spinning at periods between 1 and 50 ms. The sensitivity of our measurement was 20 mJy (5 × rms noise).

No pulsar was detected beyond 20 mJy. There is either no pulsar at all, or it is too faint, too slow, or not directed towards us. The northern area of G 18.95–1.1 ($b > -1°$) was also included in the pulsar survey at 1400 MHz by Clifton and Lyne (1986). No object was found.

In addition to our pulsar search, we also requested X-ray observations on board of EXOSAT, which would provide information also on neutron stars. The observations were scheduled but the satellite broke before that day.

No peculiar emission line stellar object is known in the central region (see Fig. 6) down to $m_{ph} = 13^m$ (CDS, Centre de Données Stellaires). A first search for a possible central star was conducted using the ESO/MPI 2.2 m telescope on La Silla. A field of 2′ × 3′ was centred on R.A. (1950) = $18^h26^m35^s$, DEC (1950) = −12°59′. Comparison of *r*-band (Thuan and Gunn, 1976) and H_α (FWHM = 5 Å) images did not show any strong emission line object down to $m_r = 17^m.5$. The spectroscopy of the brighter objects (positions marked by circles in Fig. 6) also did not reveal any peculiarity. A deeper and more extended search is in preparation.

5. Analysis

A large fraction of the radio continuum emission of G 18.95–1.1 is concentrated in a diffuse component (≈80%) at frequencies between 2.7 GHz and 10 GHz with a spectral index of $\alpha = -0.27 \pm 0.03$. This component corresponds to "crab-like" or "filled-center" SNRs. The detected integrated linear polarization

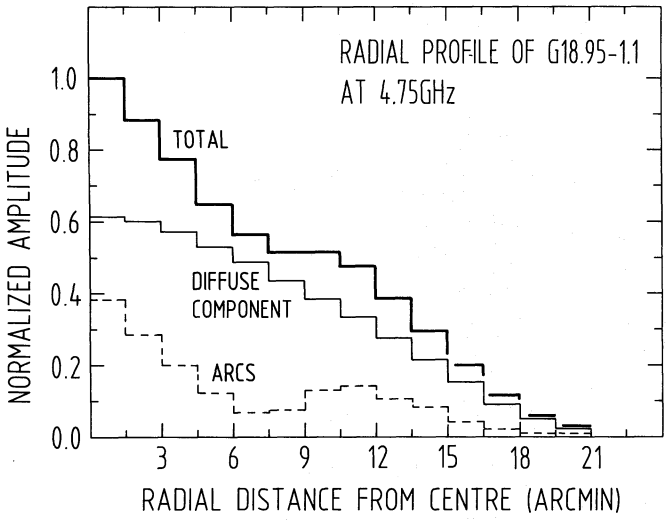

Fig. 11. The radial profile of G 18.95–1.1 at 4.75 GHz for the different components

degree of about 2.5 % is low compared with the majority of "filled-center" SNRs, but there are other exceptions (G 24.7+0.6 and G 27.8+0.6, Reich et al., 1984), which show high linear polarization only over small portions of the whole remnant.

Different from the "normal" classification of "filled-center" SNRs (Weiler, 1983) a variety of arc-like features superpose the diffuse component. If we explain these arcs as the signature of the interaction of ejecta and/or shocks with the interstellar medium, G 18.95–1.1 would be a further member of the class of composite SNRs (Weiler, 1983, 1985; Helfand and Becker, 1985) as was proposed previously by Odegard (1986), Fürst et al. (1988) and Patnaik et al. (1988). Compared with composite SNRs listed by Helfand and Becker G 18.95–1.1 is unusual because of its large "filled-center" component. The whole object is dominated by this component as can be seen from the radial profiles in Fig. 11. The arc-like features separate into a flat-spectrum central feature ($\alpha = -0.26 \pm 0.05$, similar to that of the diffuse emission) and arcs that have spectra about $\Delta\alpha = 0.1$ steeper.

The flat-spectrum central feature resembles a two-sided radio jet. Near both ends tangled structures provide some similarity of the central feature with a radio galaxy (a double-sided radio jet). However, the spectral index is much flatter than the observed values for the majority of extragalactic jets (Fomalont, 1983) and contradicts the explanation as a radio galaxy. Also no rapid steepening with increasing distance from the centre is observed. It is, therefore, reasonable to consider the central feature as galactic and physically related to G 18.95–1.1. Radio jets are also discussed in connection with galactic objects. A well studied example is the complex W 50/SS 433. Its jet structure is often explained in terms of supercritical accretion in a binary system of a neutron star and a low mass "normal" unseen companion (van den Heuvel et al., 1980; Katz, 1980; Jaroszynski et al., 1980, and others).

Let us assume that the central feature is the signature of a central jet connected with a yet unseen star-like activity. In this case one may wonder whether this central activity feeds the diffuse component (as is normally assumed for "filled-center" SNRs), where the central feature acts as a tube.

At a distance of 2 kpc the luminosity L ($10^7 - 10^{11}$ Hz) of the diffuse large-scale component is $L_{dc} = 5.4\ 10^{33}\,\mathrm{erg\,s^{-1}}$, while that of the central feature is $L_{cf} = 3\ 10^{32}\,\mathrm{erg\,s^{-1}}$ (≈ 1.6 Jy integrated flux density). If the electrons move along the main axis of the central feature and expand into the large volume of the diffuse component, the energy of the relativistic electrons varies with $(V_{cf}/V_{dc})^{1/3} \approx 1/16$, where V_{dc} is the volume of the diffuse component and V_{cf} is the volume of the central feature. Here we assumed a spherical volume of the diffuse component ($D = 20$ pc) and a cylindrical volume of the central feature ($6' \times 1'$ corresponding to 3.5×0.6 pc at a distance of 2 kpc). The electrons move along the main axis at the speed v, which is unknown, but may be close to 1/3 the speed of light as is accepted for the galactic object SS 433 (Milgrom, 1979; Hjellming and Johnston, 1981). A rough estimate of the time t_{age}, necessary to feed the diffuse emission with a sufficiently large number of relativistic electrons, is obtained assuming a constant magnetic field in both components, negligible energy losses due to radiation, and a constant acceleration efficiency of the central star-like engine. In this case $t_{age}\,(\mathrm{yr}) = (L_{dc}/L_{cf})\ \ (V_{dc}/V_{cf})^{1/3}\ \ (1.75\,\mathrm{pc}/v\,(\mathrm{pc/yr})) \approx 5000$ yr. The magnetic field in the central feature is probably larger than within the diffuse component leading to an increase of t_{age}. The acceleration efficiency has certainly declined during t_{age} and may be very low at present, in agreement with the lack of its optical and/or X-ray detection (see HEAOA-1 catalogue by Wood et al., 1984). The decline of the acceleration efficiency results in a smaller t_{age}. A more detailed investigation seems not worthwile in view of the numerous badly known parameters. $t_{age} \approx 5000$ yr may act as a first estimate of the age of G 18.95–1.1. t_{age} is sufficiently long for the electrons to be distributed almost evenly across the diffuse component. This is in agreement with the radial dependence of the volume emissivity ε derived from Fig. 2. We obtained a slight variation of ε of $\approx 50\,\%$ of the central value from the centre towards the outer boundary of G 18.95–1.1. The result is in contradiction to an expanding synchrotron nebula ($B \propto r^{-2}$, $N \propto r^{-2}$), but is in agreement with almost constant magnetic field and density of relativistic electrons across the diffuse component.

The relativistic electrons filling the volume of the diffuse centrally peaked component are confined by the outer shock, possibly represented by the steep-spectrum arcs. It is unclear whether this outer boundary is formed by the classical evolution of the SNR shock (Cox, 1972) or by the stellar wind of the progenitor star (Tomisaka et al., 1981). In case of the expansion of a blast wave the age of the remnant may be given by the equation $R_{SNR}\,(\mathrm{pc}) = 12.9\ (\varepsilon_0/n_0)^{1/5}\ t_4^{2/5}$ (Cox, 1972), where ε_0 is the initial explosion energy in units of $0.75\ 10^{51}$ erg (here $\varepsilon_0 = 1$), n_0 is the ambient density (here $n_0 = 1.5\,\mathrm{cm^{-3}}$), and t_4 is the age of the remnant in 10^4 yr. We obtain $t \approx 6500$ yr. However, the internal pressure may be affected by the central activity, decreasing this age.

In case of a stellar wind bubble created prior to the supernova explosion (density in the bubble $\approx 10^{-2}\,\mathrm{cm^{-3}}$, see Weaver et al., 1977) the expansion of the remnant is significantly faster. If the ejecta move undecelerated at a velocity of $\approx 4000\,\mathrm{km\,s^{-1}}$, they reach the boundary within ≈ 2000 yr.

Presumably, the age of G 18.95–1.1 is a few thousand years.

6. Concluding remarks

The new observations have demonstrated that the galactic object G 18.95–1.1 is a composite supernova remnant. Most of the radio emission is concentrated in a large-scale diffuse component. A small fraction ($\approx 20\,\%$) of the total emission is visible as arc-like features. One of these features is located in the direction of the geometrical centre of G 18.95–1.1 and has been shown to be

different from the other arc-like structures: The radio spectral index is flatter than that of the other arcs, and the morphology resembles a two-sided radio jet. It may be that this radio feature is located at the geometrical centre of the remnant and is physically related to a possible central star-like activity.

However, no pulsar was found and no peculiar optical object was identified as a possible active star-like source. X-ray observations are highly necessary in order to provide more insight into the nature of the central feature and to clarify the existence of a central compact source.

From H I spectral line observations we estimated the distance to G 18.95–1.1 to 2 kpc. At this distance the size of the remnant is 20 pc. The age was estimated to a few 10^3 yr.

References

Baars, J.W.M., Genzel, R., Pauliny-Toth, I.I.K., Witzel, A.: 1977, *Astron. Astrophys.* **61**, 99

Beichman, C.A., Neugebauer, G., Habing, H.J., Clegg, P.E., Chester, T.J. (eds.): 1985, IRAS Explanatory Supplement

Benford, G.: 1984, *Astrophys. J.* **282**, 154

Berkhuijsen, E.M.: 1983, *Astron. Astrophys.* **120**, 147

Boulanger, F., Band, B., Albada, G.B.: 1985, *Astron. Astrophys.* **144**, L 9

Braunsfurth, E., Rohlfs, K.: 1984, *Astron. Astrophys.* **57**, 189

Clark, D.H., Caswell, J.L.: 1976, *Monthly Notices Roy. Astron. Soc.* **174**, 226

Clifton, T.R., Lyne, A.G.: 1986, *Nature* **320**, 42

Cox, D.P.: 1972, *Astrophys. J.* **178**, 159

Einasto, J.: 1978, in *The Large-Scale Characteristics of the Galaxy*, *IAU Symp.* **84**, ed. W.B. Burton, Reidel, Dordrecht, p. 451

Fomalont, E.B.: 1983, in *Astrophysical Jets*, eds. A. Ferrari, A.R. Pacholczyk, Reidel, Dordrecht, p. 37

Fürst, E., Reich, W., Reich, P., Sofue, Y., Handa, T.: 1985, *Nature* **314**, 720

Fürst, E., Reich, W., Hummel, E., Sofue, Y.: 1987, in *The Interaction of Supernova Remnants with the Interstellar Medium*, *IAU Coll.* **101**, eds. R.S. Roger, T.L. Landecker, Cambridge University Press, p. 243

Helfand, D.J., Becker, R.H.: 1985, *Nature* **313**, 118

Helfand, D.J., Becker, R.H.: 1987, *Astrophys. J.* **314**, 203

Hjellming, R.M., Johnston, K.J.: 1981, *Astrophys. J.* **246**, L 141

Jaroszynski, M., Abramowicz, M,A., Paczyński, B.: 1980, *Acta Astron.* **30**, 1

Katz, J.I.: 1980, *Astrophys. J.* **236**, L 127

Kerr, F.J.: 1968, in *Nebulae and Interstellar Matter*, eds. B.M. Middlehurst, L.H. Aller, The Univ. Chicago Press, p. 575

Manchester, R.N., Taylor, J.N.: 1981, *Astron. J.* **86**, 1953

Milne, D.K.: 1979, *Australian J. Phys.* **32**, 83

Milgrom, M.: 1979, *Astron. Astrophys.* **76**, L 3

Odegard, N.: 1986, *Astron. J.* **92**, 1372

Ostriker, J.P., Caldwell, J.A.R.: 1978, in *The Large-Scale Characteristics of the Galaxy*, *IAU Symp.* **84**, ed. W.B. Burton, Reidel, Dordrecht, p. 441

Patnaik, A.R., Velusamy, T., Venugopal, U.R.: 1988, *Nature* **332**, 136

Reich, W., Fürst, E., Sofue, Y.: 1984, *Astron. Astrophys.* **133**, L 4

Reich, W., Fürst, E., Reich, P., Sofue, Y., Handa, T.: 1986, *Astron. Astrophys.* **155**, 185

Schmidt, M.: 1965, in *Stars and Stellar Systems V*, eds. A. Blaauw, M. Schmidt, Publ. Univ. Chicago Press

Sofue, Y., Reich, W.: 1979, *Astron. Astrophys. Suppl.* **38**, 251

Thuan, T.X., Gunn, J.E.: 1976, *Publ. Astron. Soc. Pacific* **88**, 543

Tomisaka, K., Habe, A., Ikeuchi, S.: 1981, *Astrophys. Space Sci.* **78**, 273

Turtle, A.J., Pugh, J.F., Kenderdine, S., Pauliny-Toth, I.I.K.: 1962, *Monthly Notices Roy. Astron. Soc.* **124**, 297

van den Heuvel, E.P.J., Ostriker, J.P., Petterson, J.A.: 1980, *Astron. Astrophys.* **81**, L 7

Weaver, R., McCray, R., Castor, J.: 1977, *Astrophys. J.* **218**, 377

Weiler, K.W.: 1983, *Observatory* **103**, 85

Weiler, K.W.: 1985, in *The Crab Nebula and Related SNRs*, eds. M.S. Kafatos, R.B.C. Henry, Cambridge University Press, p. 265

Weiler, K.W., Panagia, N.: 1980, *Astron. Astrophys.* **90**, 269

Wood, K.S., Meekins, J.F., Yentis, D.J., Smathers, H.W., McNutt, D.P., Bleach, R.D., Byram, E.T., Chubb, T.A., Friedman, H., Meidav, M.: 1984, *Astrophys. J. Suppl.* **56**, 507